



**Calhoun: The NPS Institutional Archive**

---

Faculty and Researcher Publications

Faculty and Researcher Publications Collection

---

1972

# Hydrodynamic Loads Induced By Earthquakes

Garrison, C.J.

---

<http://hdl.handle.net/10945/48941>



Calhoun is a project of the Dudley Knox Library at NPS, furthering the precepts and goals of open government and government transparency. All information contained herein has been approved for release by the NPS Public Affairs Officer.

**Dudley Knox Library / Naval Postgraduate School**  
**411 Dyer Road / 1 University Circle**  
**Monterey, California USA 93943**

<http://www.nps.edu/library>

THIS IS A PREPRINT --- SUBJECT TO CORRECTION

## Hydrodynamic Loads Induced By Earthquakes

By

C. J. Garrison and R. B. Berklite, Naval Postgraduate School

Offshore Technology Conference on behalf of the American Institute of Mining, Metallurgical, and Petroleum Engineers, Inc., American Association of Petroleum Geologists, American Institute of Chemical Engineers, American Society of Civil Engineers, American Society of Mechanical Engineers, Institute of Electrical and Electronics Engineers, Inc., Marine Technology Society, Society of Exploration Geophysicists, and Society of Naval Architects & Marine Engineers.

This paper was prepared for presentation at the Fourth Annual Offshore Technology Conference held in Houston, Tex., May 1-3, 1972. Permission to copy is restricted to an abstract of not more than 300 words. Illustrations may not be copied. Such use of an abstract should contain conspicuous acknowledgment of where and by whom the paper is presented.

### ABSTRACT

When bottom mounted structures of large displacement are immersed in the sea, earthquake induced hydrodynamic loads may become important design factors. Specifically, as the earth oscillates, a bottom mounted structure is forced to describe time dependent motion in an otherwise still fluid. As a result, hydrodynamic loads in addition to the inertial loads of the structure itself are induced. In this paper, a theoretical approach to the calculation of these hydrodynamic loads is outlined and numerical results are presented for several submerged configurations. Practical geometries considered include a submerged oil storage tank configuration and a conical configuration as has been proposed for offshore drilling rig designs for deployment in the Arctic. Also, computations were carried out for a sphere and vertical circular cylinder and various comparisons with classical results are made.

Numerical results for these submerged structures are presented in the form of a dimensionless hydrodynamic load parameter or added mass coefficient. Results corresponding to a number of different water depths are presented to show the rather sizable effect of the relative water depth on the hydrodynamic

force. It is shown that for typical earthquake frequencies, the effect of the free water surface is to reduce the hydrodynamic loads in comparison to the corresponding infinite depth values.

Experimental results obtained by vibration testing are presented for a submerged sphere and a vertical circular cylinder. These results show excellent agreement with the theoretical results.

### INTRODUCTION

Principal attention in earthquake engineering has been given to the generation of tsunami waves, the shoreline run-up and damage caused by these waves, as well as the damage to dry land structures caused by strong ground motion. With the increased deployment of large submerged structures, an additional facet of this important problem has come to light. Namely, if a large bottom mounted structure submerged in the ocean is excited by oscillatory ground motion, hydrodynamic loads in addition to its own inertia forces come into play. As the structure is caused to move through the water, hydrodynamic forces which are dependent upon the size and shape of the structure as well as the water depth and frequency of oscillation arise. On account of the large density of water, these forces are

References and illustrations at end of paper.

often quite large and have considerable influence on the structural design.

When an object is accelerated through a fluid there are, in general, two types of forces that are recognized, one being a drag component and a second, the inertial component. The nature of the flow produced by the time dependent motion of the immersed rigid object and the relative contribution of these two components of force is generally considered to be strongly dependent on the amplitude of the relative fluid motion in comparison to the characteristic lineal dimension of the object. For example, Keulegan and Carpenter [1] found that, for harmonic motion of the fluid past a fixed circular cylinder, major flow separation did not occur and the forces were well represented by potential flow values provided the amplitude of the motion was less than about a half diameter. If the amplitude of the motion is small enough the fluid does not move in one direction far enough for separation and wake development to occur and, accordingly, an inviscid flow analysis is a valid mathematical model.

Typical values of oscillatory ground displacement produced in earthquakes are only a few inches. Therefore, for most large engineering structures the assumption of small values of the relative amplitude of the fluid motion is well satisfied. Accordingly, the assumption of inviscid fluid motion is valid and it is justified to assume a time dependent potential flow model for analysis of the fluid motion and resulting forces.

John [2] has shown that the velocity potential associated with the harmonic motion of a rigid object immersed in a fluid with a free surface may be represented by a surface distribution of point wave sources for arbitrary values of frequency. The source distribution (or weighting) function is obtained in this formulation from the solution of an integral equation resulting from the kinematic boundary condition applied on the immersed surface. Using this technique, numerical results have been obtained, for example, for a semiellipsoid oscillating in a free surface in water of infinite depth by Kim [3], the intended application being to surface ships. Numerical results for a bottom mounted hemisphere have been presented by Garrison and Seetharama Rao [4] and results for several axisymmetric configurations by Milgram and Halkyard [5]. Garrison and Chow [6] have recently presented both theoretical and experimental results for wave forces acting on a fixed submerged oil storage tank.

In the work cited, the hydrodynamic force coefficients are represented as a function of a dimensionless frequency parameter (or equivalently, a dimensionless wave length parameter)

of the form  $\nu = \sigma^2 \bar{a}/g$  where  $\sigma$  denotes the frequency of the motion,  $\bar{a}$  denotes the characteristic lineal dimension of the submerged object and  $g$  denotes the gravitational constant. (This dimensionless parameter is essentially a form of the Froude number.) In all cases, however, the theory has a fundamental limitation. The source potential oscillates with a wave length inversely proportional to the dimensionless frequency  $\nu$  and, consequently, a reasonable partition size of the immersed surface limits the validity of the numerical scheme to small to moderate values of frequency. Specifically, it is the experience of the authors, using the Haskind's relations [7] and an energy balance for purposes of checking accuracy, that results can be obtained with reasonable accuracy up to about  $\nu = 2.0$ . Beyond this, the accuracy of the numerical results becomes questionable.

Although the range  $\nu = 0$  to about 2.0 includes most applications in ship hydrodynamics and wave forces acting on large structures, the frequencies encountered in earthquake excitation corresponds to rather large values of  $\nu$  in the case of large structures. Accordingly, an alternate method which includes the effect of the free surface and bottom on the hydrodynamic forces and is valid for large values of the dimensionless frequency  $\nu$  is required. Therefore, the work described herein is directed toward obtaining numerical results for objects of arbitrary shape for the asymptotic case of very large values of  $\nu$ , i.e., for the infinite Froude number case.

High frequency added mass coefficients for two-dimensional shapes oscillating on a free surface have been presented in a series of papers by Landweber et al. [8], [9], [10]. The motivation for this work was to provide hydrodynamic coefficients for two-dimensional ship forms. For three-dimensional objects the only results known to the author are those of Waugh and Ellis [11] for the case of a sphere in infinite depth water. Their theoretical method consisted of using successive image doublets to account for the effect of the free surface. However, the case of vertical motion only was studied and their method was limited to a sphere.

In the present paper the theoretical formulation of the forces acting on a rigid object of arbitrary shape is presented. The effect of the bottom and free surface is taken into consideration and the force coefficient is shown to depend on a frequency of oscillation parameter. The problem is first formulated for arbitrary values of the frequency and the asymptotic form of the solution for both large and small values of the frequency is discussed. A computer method for numerical evaluation of the force coefficient for submerged objects of arbitrary shape is discussed and numerical

results are presented for a number of specific geometric shapes including a circular cylinder and sphere. Also, numerical results are generated for a possible ice breaker-drilling rig configuration for deployment in the Arctic and a submerged oil storage tank. High frequency experimental results are presented for a vertical circular cylinder and submerged sphere and compared with the theoretical results.

THEORY

The geometry involved in the problem under consideration is shown in Fig. 1. A rigid object of arbitrary shape having characteristic lineal dimension  $\bar{a}$  is submerged to a depth  $\bar{d}$  in water of depth  $\bar{h}$  and caused to move in a small amplitude harmonic motion. The instantaneous motion of the rigid object is specified by the lineal velocity  $\vec{U}$  and angular velocity  $\vec{\Omega}$ . The object may intersect the bottom or free surface.

Assuming an unseparated, incompressible and irrotational flow, a velocity potential  $\phi(\bar{x}_1, \bar{x}_2, \bar{x}_3, t)$  defined by

$$\vec{q} = \vec{\nabla}\phi \tag{1}$$

where  $\vec{q}$  denotes the fluid velocity vector, may be introduced and must satisfy the continuity equation,

$$\nabla^2\phi = 0 \tag{2}$$

within the fluid region. (The bars over the spatial variables denote dimensional quantities)

On the rigid bottom surface described by  $\bar{x}_2 = -\bar{h}$  the fluid velocity in the vertical direction must vanish and, accordingly, the corresponding kinematic boundary condition on the velocity potential is

$$\frac{\partial\phi}{\partial\bar{x}_2}(\bar{x}_1, -\bar{h}, \bar{x}_3, t) = 0 \tag{3}$$

The velocity of a point on the immersed surface is given by

$$\vec{V} = \vec{U} + \vec{\Omega} \times \vec{r} \tag{4}$$

where  $\vec{r}$  denotes the position vector as shown in Fig. 1. The appropriate kinematic and dynamic boundary condition on the immersed surface, therefore, takes the form

$$\frac{\partial\phi}{\partial\bar{n}}(x_1, x_2, x_3, t) = \vec{V} \cdot \vec{n} \tag{5}$$

where  $\vec{n} = \vec{i}n_1 + \vec{j}n_2 + \vec{k}n_3$  denotes the unit normal vector on the surface and is directed outward into the fluid region.

Assuming the amplitude of the motion of the object to be small, the kinematic and dynamic boundary condition applied at the free surface may be linearized to give

$$\frac{\partial\phi}{\partial\bar{x}_2}(\bar{x}_1, 0, \bar{x}_3, t) + \frac{\partial^2\phi}{\partial t^2}(\bar{x}_1, 0, \bar{x}_3, t) = 0 \tag{6}$$

Furthermore, if the object oscillates with frequency  $\sigma$ , the time dependence of the velocity potential may be separated and written as  $\text{Re}[\phi(x_1, x_2, x_3)e^{-i\sigma t}]$  where  $\text{Re}$  denotes the real part. In which case Eq. (6) becomes

$$\frac{\partial\phi}{\partial\bar{x}_2}(\bar{x}_1, 0, \bar{x}_3) - \frac{\sigma^2}{g}\phi(\bar{x}_1, 0, \bar{x}_3) = 0 \tag{7}$$

Thus, when  $\sigma$  is very large, the free surface boundary condition takes the form

$$\phi(\bar{x}_1, 0, \bar{x}_3) = 0 \tag{8}$$

and when  $\sigma$  is very small the free surface appears as a rigid boundary as described by

$$\frac{\partial\phi}{\partial\bar{x}_2}(\bar{x}_1, 0, \bar{x}_3) = 0 \tag{9}$$

If consideration is restricted to either of the boundary conditions Eq. (8) or Eq. (9) the velocity potential may be written as the sum

$$\phi(\bar{x}_1, \bar{x}_2, \bar{x}_3, t) = W_i(t) \phi_i(x_1, x_2, x_3), \tag{10}$$

$i = 1, 2, \dots, 6$

where each term in the sum represents the potential associated with the  $i^{\text{th}}$  component of body motion. ( $i = 1, 2, 3$  refers to lineal motion components in the  $x_1, x_2, x_3$  directions, respectively, and  $i = 4, 5, 6$  refers to the angular motion components about the  $\bar{x}_1, \bar{x}_2, \bar{x}_3$  axes, respectively.) The time dependent function  $W$  is defined as

$$\left. \begin{aligned} W_i(t) &= U_i(t) \bar{a} \\ W_{i+3}(t) &= \Omega_i(t) \bar{a}^2 \end{aligned} \right\} i = 1, 2, 3 \tag{11}$$

the symbols  $U_i$  and  $\Omega_i$  denoting the components of the lineal and angular velocity vectors of the body,  $\vec{U}$  and  $\vec{\Omega}$ , respectively. The potentials  $\phi_i$  are dimensionless quantities.

It is important to note that the application of either of the two boundary conditions, Eqs. (8) and (9), makes the problem homogeneous in time. Consequently, the assumption of harmonic motion may be relaxed and the functions  $W_i(t)$  may be allowed to be arbitrary functions. This is fortunate since earthquake excitation is not harmonic but rather a high frequency random vibration.

Substituting Eq. (10) into Eqs. (2), (3), (5) and (8) or (9) and introducing the dimensionless variables defined as

$$x_i = \bar{x}_i/\bar{a}, \quad h = \bar{h}/\bar{a}, \quad d = \bar{d}/\bar{a} \tag{12}$$

yields the boundary value problem for  $\phi_i$  ( $i = 1, 2, \dots, 6$ ) as:

$$\nabla^2 \phi_1(x_1, x_2, x_3) = 0$$

$$\phi_1(x_1, 0, x_3) = 0, \quad (\sigma \rightarrow \infty)$$

$$\text{or, } \frac{\partial \phi_1(x_1, 0, x_3)}{\partial x_2} = 0, \quad (\sigma \rightarrow 0) \quad (13 \text{ a-e})$$

$$\frac{\partial \phi_1(x_1, -h, x_3)}{\partial x_2} = 0$$

$$\frac{\partial \phi_1(x_1, x_2, x_3)}{\partial n} = m_i$$

where

$$\begin{aligned} m_1 &= n_i, \quad i = 1, 2, 3 \\ m_4 &= (x_2 + d)n_3 - x_3 n_2 \\ m_5 &= x_3 n_1 - x_1 n_3 \\ m_6 &= x_1 n_2 - (x_2 + d)n_1 \end{aligned} \quad (14 \text{ a-d})$$

The boundary conditions (13b) and (13c) represent two different possibilities on the free surface, the first being the high frequency condition and the second the rigid boundary condition. In as much as the method of solution involving either boundary condition is similar, both solutions are developed simultaneously in the following.

#### Green's Function Solution

The solution to the boundary value problem (13) may be carried out by use of a Green's function. The Green's function represents the potential for a point source and these sources are distributed over the immersed surface according to the distribution function  $f(\xi_1, \xi_2, \xi_3)$ . According to this concept the potential  $\phi$  may be written as

$$\phi_1(x_1, x_2, x_3) = \frac{1}{4\pi} \iint_S f_i(\xi_1, \xi_2, \xi_3) G(x_1, x_2, x_3; \xi_1, \xi_2, \xi_3) dS \quad (15)$$

where  $(\xi_1, \xi_2, \xi_3)$  denotes a point on the immersed surface,  $G$  denotes the Green's function and  $dS = d\bar{S}/\bar{a}^2$  denotes the surface area element made dimensionless with the characteristic body dimension  $\bar{a}$ .

In order that Eq. (15) represent a solution to Eqs. (13) it is necessary that  $G$  satisfy the equation

$$\begin{aligned} \nabla^2 G(x_1, x_2, x_3; \xi_1, \xi_2, \xi_3) &= \\ \delta(x_1 - \xi_1) \delta(x_2 - \xi_2) \delta(x_3 - \xi_3), \end{aligned} \quad (16)$$

where  $\delta(x)$  denotes the Dirac delta function, as well as boundary conditions (13d) and (13b) or (13c).

The Green's function satisfying Eq. (16) as well as Eq. (13b) and (13d) is obtained by use of successive images as depicted in Fig. 2 and is given by

$$\begin{aligned} G(x_1, x_2, x_3; \xi_1, \xi_2, \xi_3) &= \frac{1}{R} - \frac{1}{R_1} \\ &+ \sum_{n=1}^{\infty} [(-1)^n \left(\frac{1}{R_{2n}} + \frac{1}{R_{4n}}\right) + (-1)^{n+1} \left(\frac{1}{R_{3n}} + \frac{1}{R_{5n}}\right)] \end{aligned} \quad (17)$$

The corresponding form of  $G$  satisfying the rigid boundary condition Eq. (13c) ( $\sigma = 0$  on  $x_2 = 0$ ) is also obtained by successive images and is similar to Eq. (17) except that all of the sources have positive strengths. For this case, the Green's function takes the form

$$\begin{aligned} G(x_1, x_2, x_3; \xi_1, \xi_2, \xi_3) &= \frac{1}{R} + \frac{1}{R_1} \\ &+ \sum_{n=1}^{\infty} \left(\frac{1}{R_{2n}} + \frac{1}{R_{3n}} + \frac{1}{R_{4n}} + \frac{1}{R_{5n}}\right) \end{aligned} \quad (18)$$

where in both Eq. (17) and (18)

$$\begin{aligned} \omega &= \sqrt{(x_1 - \xi_1)^2 + (x_3 - \xi_3)^2} \\ R &= \sqrt{\omega^2 + (x_2 - \xi_2)^2} \\ R_1 &= \sqrt{\omega^2 + (x_2 + \xi_2)^2} \\ R_{2n} &= \sqrt{\omega^2 + (x_2 - 2nh - \xi_2)^2} \\ R_{3n} &= \sqrt{\omega^2 + (x_2 + 2nh + \xi_2)^2} \\ R_{4n} &= \sqrt{\omega^2 + (x_2 - 2nh - \xi_2)^2} \\ R_{5n} &= \sqrt{\omega^2 + (x_2 - 2nh + \xi_2)^2} \end{aligned} \quad (19)$$

Since  $G$  satisfies Eq. (13a-e) the potential  $\phi_1$  as given by Eq. (15) must also satisfy these conditions. Thus, it remains to select the function  $f$  such that Eq. (13e) is satisfied. Application of this boundary condition yields the following integral equation

$$\begin{aligned} -f_1(x_1, x_2, x_3) &+ \frac{1}{2\pi} \iint_S f_i(\xi_1, \xi_2, \xi_3) \frac{\partial G(x_1, x_2, x_3; \xi_1, \xi_2, \xi_3)}{\partial n} dS \\ &= 2m_i(x_1, x_2, x_3), \quad i = 1, 2, \dots, 6 \end{aligned} \quad (20)$$

which is to be solved for  $f(\xi_1, \xi_2, \xi_3)$ . Because of the form of  $G$ , Eq. (20) is rather complex and it is therefore necessary to carry out the solution numerically. Since the source strength  $f$  is a well-behaved function, the immersed surface may be partitioned into  $N$  area elements of size  $\Delta S_i$  and the integral in Eq. (20) written as the sum

$$-f_{n_i} + f_{n_j} \alpha_{ij} = 2m_{n_i}, \quad n = 1, 2, \dots, 6 \quad (21)$$

where  $i, j = 1, 2, \dots, N$  and  $n$  refers to the six possible modes of motion of the object. It follows from Eq. (20) that

$$\alpha_{ij} = \frac{1}{2\pi} \iint_{\Delta S_j} \frac{\partial G}{\partial n} (x_{1_i}, x_{2_i}, x_{3_i}; \xi_1, \xi_2, \xi_3) dS \quad (22)$$

The function  $\partial G/\partial n$  is obtained in a straightforward manner by differentiation of Eq. (17) or (18).

Once the coefficient matrix  $\alpha_{ij}$  is obtained from Eq. (22) a standard digital computer subroutine may be used to invert the matrix equation, Eq. (21), to obtain the source strength  $f$  at points on the immersed surface. For purposes of evaluation of  $G$  and  $\partial G/\partial n$  by use of (17) and (18) it was found that about 15 terms were adequate. The data presented herein, however, were obtained using 30 terms.

Hydrodynamic Forces and Moments

The dynamic fluid pressure is obtained from the linearized form of Bernoulli's equation as

$$P = -\rho \frac{\partial \phi}{\partial t} \quad (23)$$

Corresponding to the  $i^{th}$  component of body motion, the pressure is obtained by use of Eq. (10) as

$$P_i = -\rho \dot{w}_i \phi_i \quad (\text{no sum}) \quad i = 1, 2, \dots, 6 \quad (24)$$

The pressure may be written in dimensionless coefficient form as

$$P_i(x_1, x_2, x_3) = \frac{P_i(x_1, x_2, x_3)}{\rho \dot{w}_i} = -\phi_i(x_1, x_2, x_3), \quad i = 1, 2, \dots, 6 \quad (25)$$

The hydrodynamic force acting on the object is finally obtained by carrying out the integration of the pressure over the immersed surface. Using Eq. (24) the force vector associated with the  $j^{th}$  component of body motion is

$$\vec{F}_j = -a^2 \iint_S P_j \vec{n} dS, \quad j = 1, 2, \dots, 6 \quad (26)$$

The corresponding result for the moment vector is

$$\vec{M}_j = -a^3 \iint_S P_j \vec{r} \times \vec{n} dS, \quad j = 1, 2, \dots, 6 \quad (27)$$

Using Eq. (24) as well as the definition of  $m_j$  as given in Eq. (14), the  $i^{th}$  component of force associated with the  $j^{th}$  component of motion is given in dimensionless coefficient form as

$$A_{ij} = \frac{F_{ij}}{\rho a^2 \dot{w}_j} = \iint_S \phi_j m_i dS, \quad \begin{cases} i = 1, 2, 3 \\ j = 1, 2, \dots, 6 \end{cases} \quad (28)$$

and the corresponding expression for moment is

$$A_{ij} = \frac{M_{ij}}{\rho a^3 \dot{w}_j} = \iint_S \phi_j m_i dS, \quad \begin{cases} i = 4, 5, 6 \\ j = 1, 2, \dots, 6 \end{cases} \quad (29)$$

where  $W$  is defined by Eq. (11).

Equations (28) and (29) define the inertia (or added mass) tensor having 36 elements. The dimensionless coefficients  $A_{ij}$  defined by Eq. (28) represent the dimensionless force coefficient and Eq. (29) represents the dimensionless moment coefficient. These coefficients are generally referred to as added mass (or moment of inertia) coefficients. Although these coefficients are made dimensionless by use of  $a$  in the definitions (28) and (29), there are cases, depending on the body geometry, where other length scales are more appropriate. It is also standard practice in many cases to use the displaced fluid volume. However, in all numerical results presented herein the definition of  $A_{ij}$  is specified on the figure so that although the definitions vary, no confusion should result.

For purposes of numerical evaluation of the coefficients given in Eqs. (28) and (29) the integrals may be written as summation

$$A_{ij} = (\phi_j m_i)_k \Delta S_k, \quad \begin{matrix} i, j = 1, 2, \dots, 6 \\ k = 1, 2, \dots, N \end{matrix} \quad (30)$$

However, in order to apply Eq. (30) it is necessary to first evaluate  $\phi_j$  at all of the nodal points on the immersed surface. For this purpose the surface integration in Eq. (15) is also converted to the summation

$$(\phi_j)_k = \beta_{k\ell} (f_j)_\ell, \quad \begin{matrix} j = 1, 2, \dots, 6 \\ k, \ell = 1, 2, \dots, N \end{matrix} \quad (31)$$

where

$$\beta_{k\ell} = \frac{1}{4\pi} \iint_{\Delta S_\ell} G(x_{1_k}, x_{2_k}, x_{3_k}; \xi_1, \xi_2, \xi_3) dS \quad (32)$$

Once Eq. (32) is evaluated, the summation indicated in Eq. (31) may be carried out to determine  $\phi_j$  at all nodal points on the immersed surface. The coefficients  $A_{ij}$  are then obtained by use of Eq. (30).

Although there are 36 possible added mass coefficients, many are zero on account of symmetry and most off-diagonal elements are small. Also, even for a body of arbitrary shape  $A_{ij}$  is symmetrical so that at most only 21 of the coefficients need be evaluated. That is, Eq. (13e) along with Eq. (28) and (29) gives

$$A_{ij} = \iint_S \phi_j m_i dS = \iint_S \phi_j \frac{\partial \phi_i}{\partial n} dS \quad (33)$$

By use of the Green's theorem applied to the fluid region external to the body, it can be shown that

$$\iint_S \phi_j \frac{\partial \phi_1}{\partial n} dS = \iint_S \phi_1 \frac{\partial \phi_j}{\partial n} dS \quad (34)$$

since on the free surface either  $\phi = 0$  or  $\partial\phi/\partial n = 0$  (depending on the boundary condition being enforced) and  $\partial\phi/\partial n = 0$  on the bottom. Therefore, in view of Eq. (34) and (33) it is apparent that the added mass tensor is symmetrical,

$$A_{ij} = A_{ji} \quad (35)$$

#### EXPERIMENTAL APPROACH

Experiments were conducted to determine the added mass coefficient of a circular cylinder and a sphere in proximity of a free surface and rigid bottom. The basic experimental approach consisted of mounting the test object on flexible beams and measuring its natural frequency in air and water. The reduction in natural frequency when placed in water was then related to the added mass of the water.

The test rig used to determine the added mass coefficient corresponding to the horizontal motion of a vertical circular cylinder and sphere is shown in Fig. 3 and 4. The sphere was mounted in this test rig on a thin 6 inch long by 2 inch chord vertical strut. Two large steel channels were placed perpendicular to each other and welded to a 1/2-inch steel plate to form a rigid support for the spring-mass system. These channels were supported at four points on the top edge of a shallow, water-tight box (24" x 70" x 48"). The cylinder and sphere, mounted on a pair of flexible beams, was bolted to this supporting structure as shown in Fig. 3. (The sphere is not shown.)

Four strain gages were mounted on the top end of one of the flexible beams and connected into a Wheatstone bridge. The bridge was then connected to a carrier preamplifier and the frequency of the bridge output was measured by use of a Monsanto programmable counter-timer. A ten second duration was set on the counter-timer and, depending on the depth of water and test object, the readings ranged from about 110 to 180 cycles. The time duration programmed on the counter was highly accurate so that the major error in the process was considered to result from reading the number of cycles occurring in the 10 second interval to integer values. However, since the starting of the interval was random, this error was minimized by repeating each test run six times and recording the average reading. It was noted that the spread in readings from the counter was never greater than one cycle for a given configuration.

A calibration curve for the system was developed by plucking the mass (test object) in air with the addition of pre-measured weights attached to the test object. In general, the

test procedure was considered to be highly accurate and good repeatability was obtained in all cases.

The same procedure was used for the determination of the added mass coefficients for the sphere in vertical motion but a different apparatus and tank was employed. The parallel beam mount which carried the rod with attached 6 inch diameter plexiglass sphere is shown in Fig. 5 and 6. The tank used in this experiment was 4.0 ft. deep and represented, for practical purposes, an infinite depth case. The sphere was oscillated in the vertical direction.

#### DISCUSSION OF RESULTS

Theoretical and experimental values of added mass coefficients have been generated for a number of configurations and are plotted in Figs. 7 - 18. These include results for a vertical circular cylinder, a sphere, a hemispherical bottom mounted vessel, a practical submerged oil storage tank and a conically shaped tower.

The theoretical and experimental results for the added mass coefficient for a vertical circular cylinder are shown in Figs. 7 - 11. The added mass coefficient corresponding to the case of horizontal acceleration as based on the cylinder radius cubed is presented in Fig. 7 both with a free surface and with a rigid upper boundary. Results for two different grid sizes are shown, 120 and 192 effective nodal points, and little difference was found to exist. It can be seen that the computer results for the "rigid boundary" case closely follow the straight line relationship ( $\pi h$ ) representing the classical two-dimensional result. The results corresponding to the "free surface" case show that the effect of the free surface is to reduce the added mass coefficient and for larger values of  $h$  the results appear to be closely approximated by the straight line relationship ( $\pi h - 3.0$ ).

The same result in a slightly different form is presented in Fig. 8. In this figure the added mass coefficient made dimensionless in the more common manner, by use of the displaced volume  $\pi a^2 h$ , is plotted for two different grid sizes. Also, the experimental results obtained from vibration testing is presented for comparison. The results show that the effect of the free surface is to reduce the added mass coefficients and agreement between the experimental and theoretical results is shown to be excellent. On the same figure the computer results for the rigid boundary case is presented. The classical result for two-dimensional flow gives  $A_{11} = 1.0$  and, therefore, the deviation from this value gives the percentage numerical error in the computer results directly. The figure indicates a

maximum of about 3.0 per cent error at the extreme low values of  $h$ .

There is no doubt that accuracy of the computer results could be improved by means other than the most obvious: increasing the number of area elements. However, any gain in precision is generally offset by increased computer storage requirements, complexity and computer run time. The present method is considered to be quite simple and versatile with respect to configuration and yet possesses adequate accuracy for most purposes.

For the case of horizontal motion, the line of action of the horizontal force is also a parameter of interest. When the upper boundary acts as a "wall," the force acts at the center, i.e., at  $l = .5$ . However, for the free surface case the pressures are reduced near the free surface and the line of action is somewhat below center. This result is presented in Fig. 9 as obtained using 192 nodal points.

A second degree of freedom is also possible for the vertical cylinder. The cylinder may be allowed to rotate about some convenient axis with angular acceleration. In which case an added moment of inertia may be defined. Numerical results have been generated, using 192 nodal points, for this coefficient for rotation about an axis passing through the center of the cylinder at its base. These theoretical results are presented in Fig. 10. The results show that the free surface has the effect of reducing the hydrodynamic reaction when compared to the rigid boundary case. This is the expected result since the free surface tends to reduce the pressure differential near the top of the cylinder.

Finally, in order to show how the maximum pressure on the surface of the cylinder varies with depth, Fig. 11 has been prepared. In this figure the dimensionless pressure coefficient as defined by Eq. (25) is plotted for the case of horizontal acceleration. It may be noted that the classical solution corresponding to the rigid boundary case yields the maximum pressure of  $p_1 = 1.0$  over the complete length. Fig. 11 shows that the pressure corresponding to the free surface case begins at zero and appears to approach unity as the distance from the free surface and depth increase. This is the expected trend since the effect of the free surface diminishes at large distances.

Theoretical results for a sphere accelerating both horizontally and vertically are shown in Figs. 12 - 14. For the case of vertical acceleration in deep water, Fig. 12 shows experimental results obtained by vibration testing for comparison with theory and

the agreement appears to be quite good. It may be noted that the effect of the free surface is always to decrease the added mass coefficients while the proximity of a rigid boundary has the opposite effect. All of the computer results for the sphere have been generated using 264 nodal points.

The well-known classical solution for a sphere gives an added mass coefficient of .5 for the case of a fluid of infinite extent. Accordingly, as  $d$  becomes large, the coefficient plotted in Fig. 12 is expected to approach this closed form result but approximately a 4.0 per cent deviation is noted. This error is due to numerical inaccuracies and approximations used in the computer program.

The same kind of results are plotted in Fig. 13 as generated by the computer, the only difference being the finite depth,  $h = 4.0$ . The same general trends as in Fig. 12 are observed when the sphere is near the free surface; the rigid boundary results are greater than .5 while the free surface results are less than .5. However, as the depth is increased and the sphere approaches the bottom, the added mass coefficient increases in either case.

Theoretical and experimental results for the added mass coefficient in horizontal acceleration corresponding to a bottom mounted sphere is shown in Fig. 14. The experimental results were obtained by use of the test rig shown in Figs. 3 and 4. The sphere was mounted on the lower plate by use of a 6.0 inch strut and the sphere was adjusted to within .02 inches of the tank floor. It may be noted that the results show good agreement with theoretical results and have the same general trends as previous results except for the break off in  $A_{11}$  for the rigid boundary case as  $h$  becomes small. This reversal in trend is caused by the un wetting of the sphere occurring at values of  $h$  less than 2.0.

Fig. 15 presents the added mass coefficient associated with a bottom mounted hemispherical object as a function of water depth for both the rigid boundary and free surface case. The results appear somewhat similar to previous ones with the rigid boundary having the effect of increasing the added mass coefficient and the free surface having the opposite effect.

In order to demonstrate the capability of the method, computer results have been generated for two practical concrete structures. The first, shown in Fig. 16, is a conically shaped tower which may find application as a drilling rig for deployment in the Arctic. The computer results were generated using 192 effective nodal points distributed over the immersed surface.

The added mass coefficient (based on actual displaced volume) for the conically shaped tower



is presented in Fig. 16 as a function of water depth. The results for the rigid boundary case shows coefficients which are much greater than those corresponding to the free surface case. Moreover, for the free surface case the line of action of the hydrodynamic force was found to actually lie below the bottom. This rather unexpected result is caused by the fact that the pressures on the lower portion contribute to a moment opposite that induced by pressures on the upper part. In general, as the object is accelerated horizontally, positive pressures are produced on the front side while negative pressures occur on the back side. Therefore, since the pressure as well as area which contributes to a negative moment is much greater than those tending to induce a positive moment, the result is a moment tending to tip the top of the cone in the direction of the acceleration. This moment is equivalent to applying the horizontal force at a distance  $\ell$  below the bottom.

A second configuration of practical interest is the bottom mounted submerged oil storage vessel described in Fig. 17. The dimensions are made dimensionless with respect to the tank half-width. In the original design the tank width was approximately 100 feet.

The added mass coefficient based on the displaced volume both with a rigid upper boundary and with a free surface is shown in Fig. 18. Here again the results are similar to previous ones with the rigid boundary case showing an increase and the free surface case showing a decrease in added mass coefficient at smaller values of the depth. These results were generated using 236 effective nodal points distributed over the complete immersed surface.

#### CONCLUSIONS

A practical, numerical analysis has been developed using three dimensional sources and image sources to represent the flow produced during impulsive motion of large rigid structure of arbitrary shape immersed in the sea. The bottom and free surface have been taken into account and it is shown that the proximity of the free surface has a sizable effect and always tends to reduce the added mass coefficients in comparison to the rigid boundary case. The experimental results obtained by vibration testing for a sphere and cylinder were found to agree well with the theoretical results. The results are directly applicable in the determination of earthquake loading of rigid submerged and semi-submerged bottom mounted structures.

#### NOMENCLATURE

$\bar{a}$ : characteristic dimension of the body  
 $A_{1j}$ : added mass coefficient  
 $\bar{d}^{1j}$ : depth of submergence  
 $f(\xi_1, \xi_2, \xi_3)$ : source strength function

$\vec{F}$ : force vector  
 $g$ : acceleration of gravity  
 $G$ : Green's function  
 $h$ : depth of water  
 $\vec{M}$ : moment vector  
 $\vec{n}$ : unit normal vector  
 $p$ : dynamic pressure, dimensionless  
 $P$ : dynamic pressure  
 $\vec{q}$ : fluid velocity vector  
 $S$ : surface of body  
 $t$ : time  
 $\vec{U}$ : velocity of object  
 $x_1, x_2, x_3$ : coordinates  
 $v = \frac{\sigma^2 a}{g}$   
 $\xi_1, \xi_2, \xi_3$ : coordinates of a point on the surface of the object  
 $\rho$ : fluid density  
 $\sigma$ : frequency  
 $\phi$ : velocity potential, dimensionless  
 $\Phi$ : velocity potential  
 $\Omega$ : angular velocity of body

#### ACKNOWLEDGMENTS

The authors are pleased to acknowledge Mr. W. J. Talbot, Jr. of Santa Fe - Pomeroy, Inc. for suggesting the problem and for providing data relative to the submerged tank. Also, the help of Messrs. L. C. Horne, F. K. McGrath and D. H. Peters, students at the Naval Postgraduate School, in carrying out the experiments is greatly appreciated.

#### REFERENCES

- Keulegan, G. H. and Carpenter, L. H.: "Forces on Cylinders and Plates in an Oscillating Fluid," J. of Research of the National Bureau of Standards, Research Paper No. 2857, Vol. 60, No. 5, May 1958.
- John, F.: "On the Motion of Floating Bodies II," Comm. Pure Appl. Math. Vol. 3, 45-101, 1950.
- Kim, W. D.: "On the Harmonic Oscillation of a Rigid Body on a Free Surface," J. Fluid Mech., Vol. 21, 427-451.
- Garrison, C. J. and Seetharama Rao, V.: "Interaction of Waves with Submerged Objects" J. Waterways, Harbors and Coastal Engineering Div., Proc. ASCE, Vol. 97, No. WW2, May 1971.
- Milgram, J. H. and Halkyard, J. E.: "Wave Forces on Large Objects in the Sea," J. Ship Research, June 1971.
- Garrison, C. J. and Chow, P. Y.: "Forces exerted on a Submerged Oil Storage Tank by

Surface Waves," J. Waterways, Harbors and Coastal Engineering Div., Proc. ASCE (in press).

- 7. Newman, J. N.: "The Exciting Forces on Fixed Bodies in Waves," J. Ship Research, December 1962.
- 8. Landweber, L.: "Added Mass of Lewis Forms Oscillating in a Free Surface," Proc. Symposium on the Behavior of Ships in a Seaway, Netherlands Ship Model Basin, Sept. 1957.
- 9. Landweber, L. and Macagno, M.: "Added

Mass of Two-Dimensional Forms Oscillating in a Force Surface," J. Ship Research, Vol. 1, November 1957.

- 10. Landweber, L. and Macagno, M.: "Added Mass of Two-Dimensional Forms by Conformal Mapping," J. Ship Research, June 1967.
- 11. Waugh, J. G. and Ellis, A. T.: "Fluid-Free-Surface Proximity Effects on a Sphere Vertically Accelerated from Rest," J. Hydronautics, Vol. 3, No. 4, October 1969.

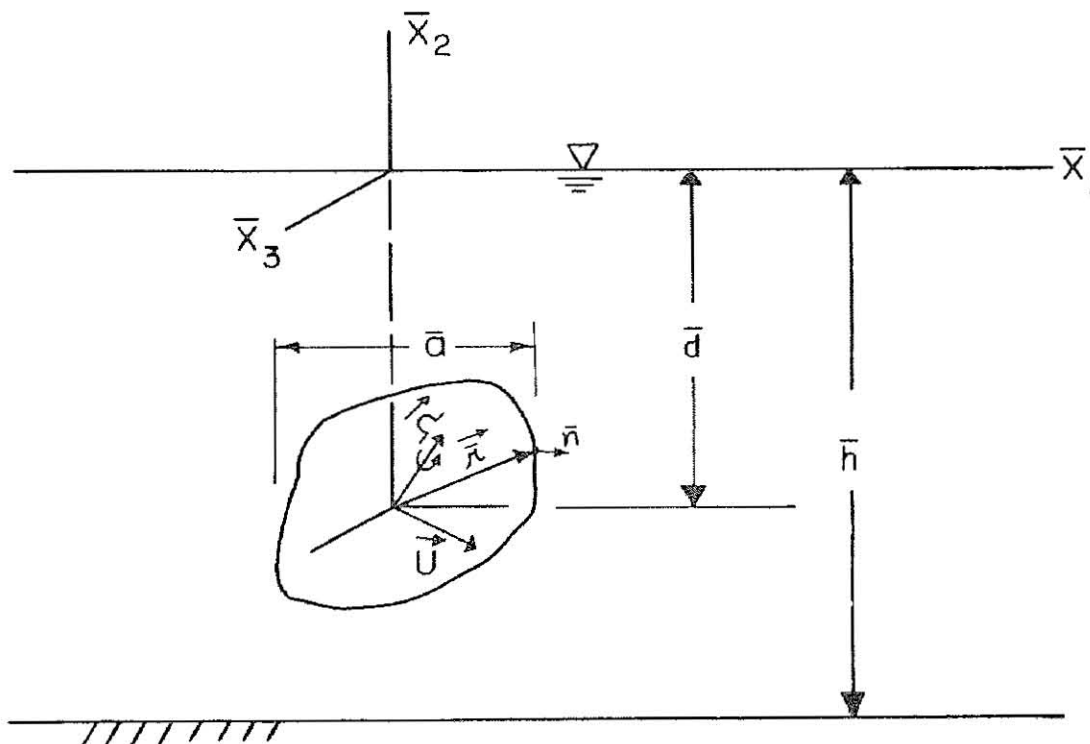


Fig. 1 - Definition of geometry.

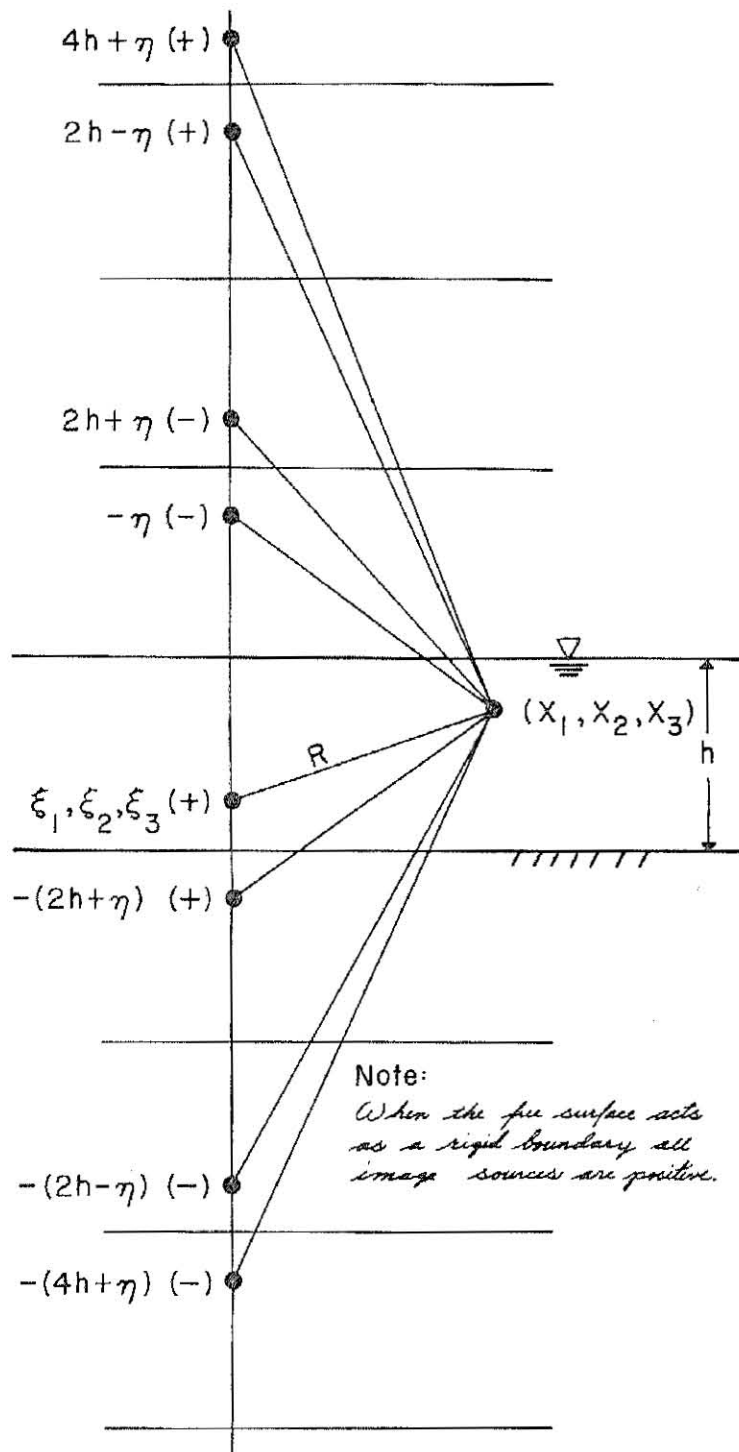


Fig. 2 - Image source layout.

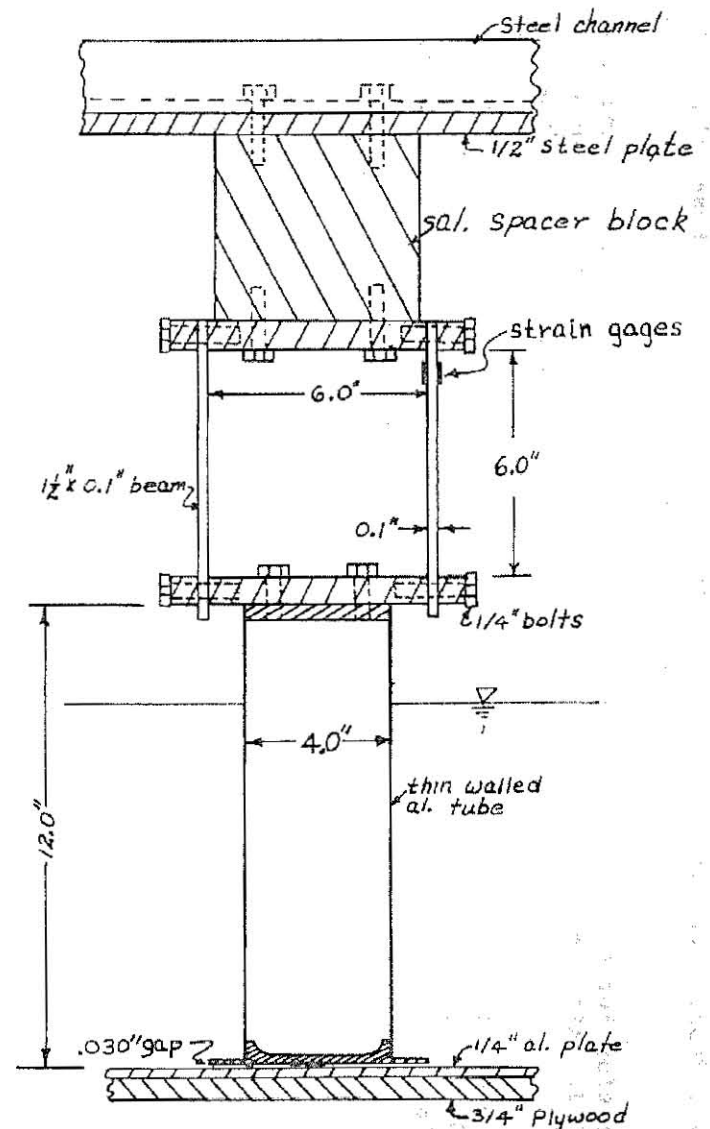


Fig. 3 - Experimental equipment.



Fig. 4 - Experimental apparatus.

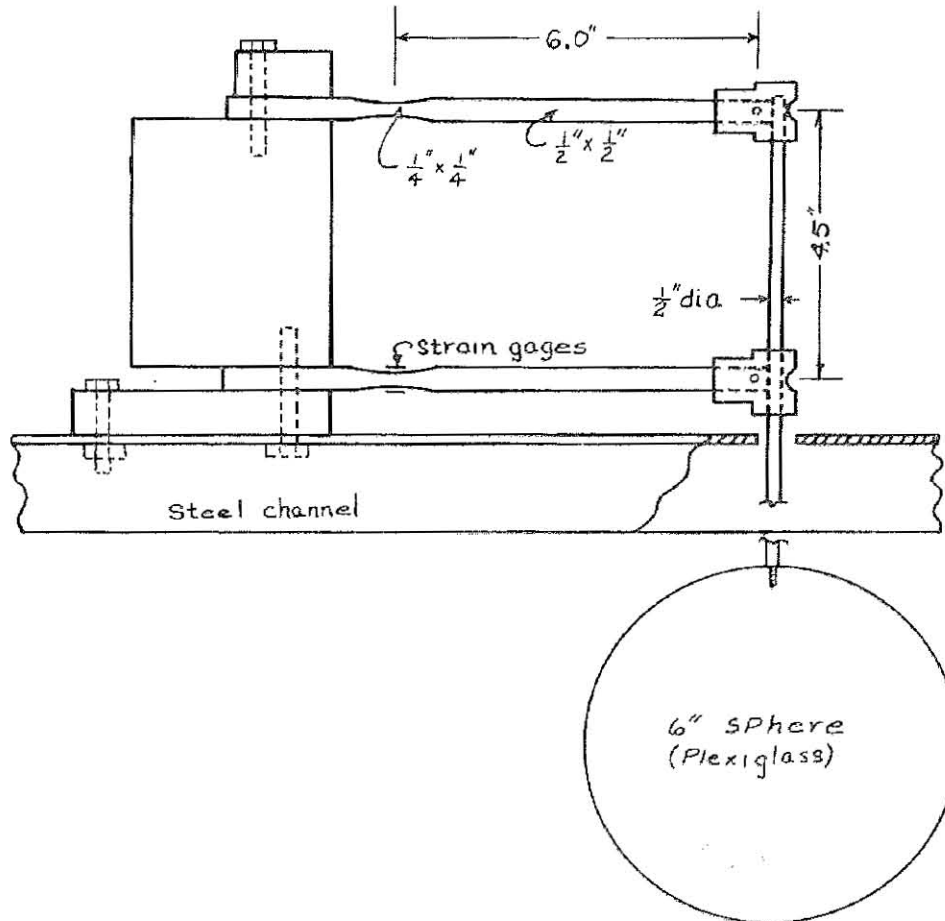


Fig. 5 - Experimental apparatus used in heave tests.

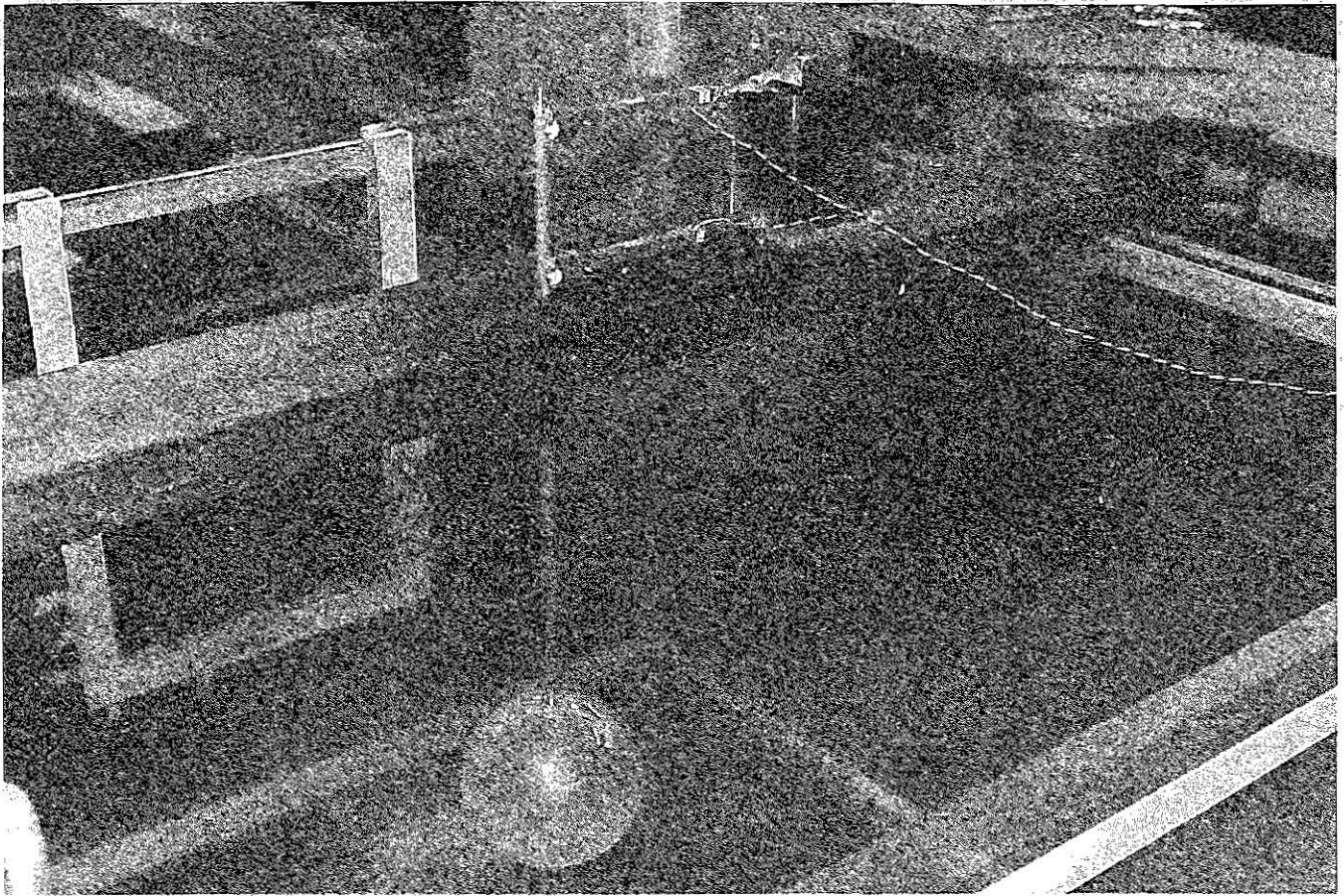


Fig. 6 - Experimental apparatus.

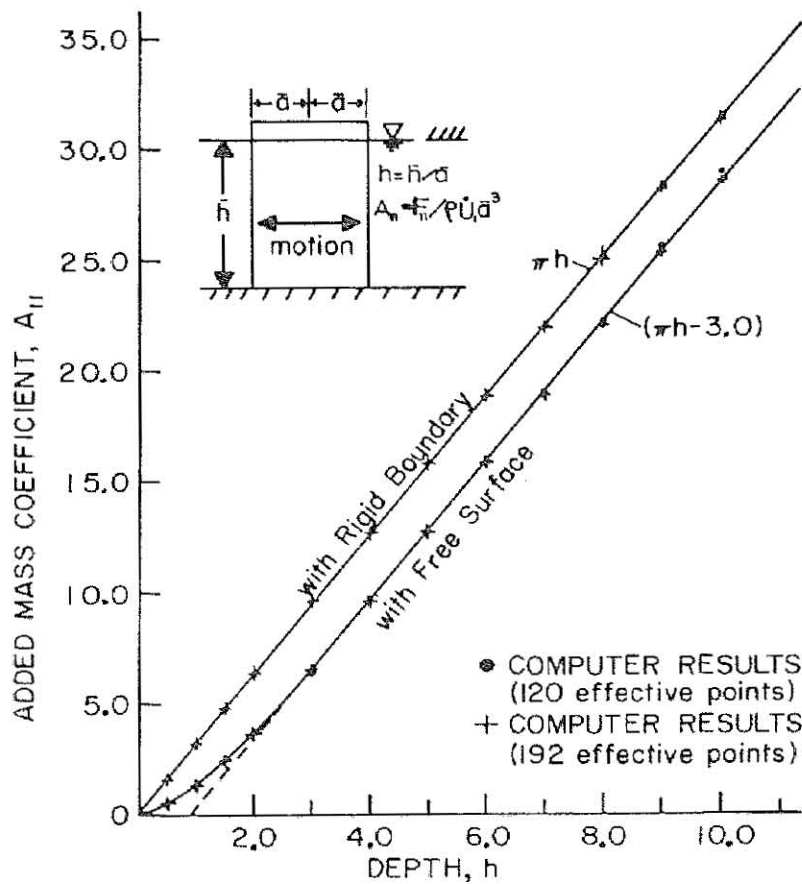


Fig. 7 - Added mass coefficient for a vertical circular cylinder.

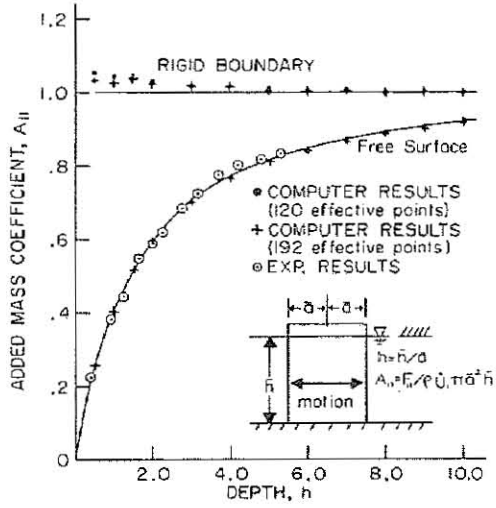


Fig. 8 - Added mass coefficient for a vertical circular cylinder.

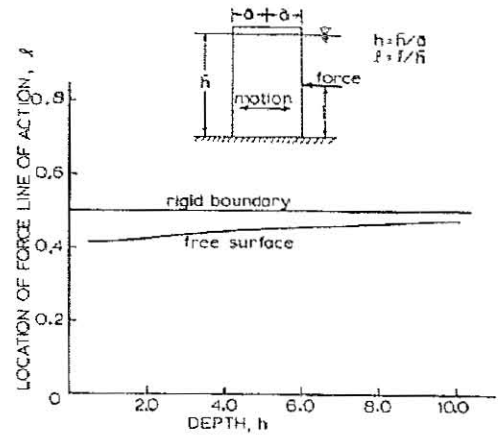


Fig. 9 - Location of effective line of action of hydrodynamic inertia force for a vertical circular cylinder.

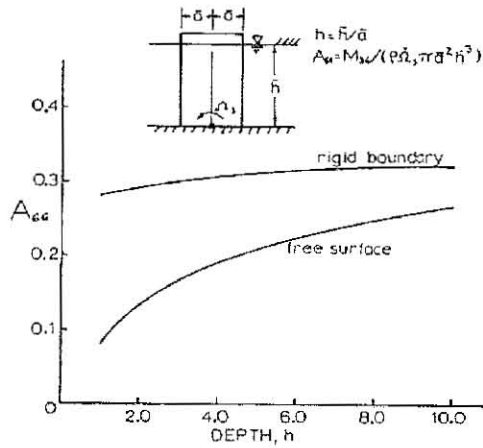


Fig. 10 - Added moment of inertia coefficient for a vertical circular cylinder.

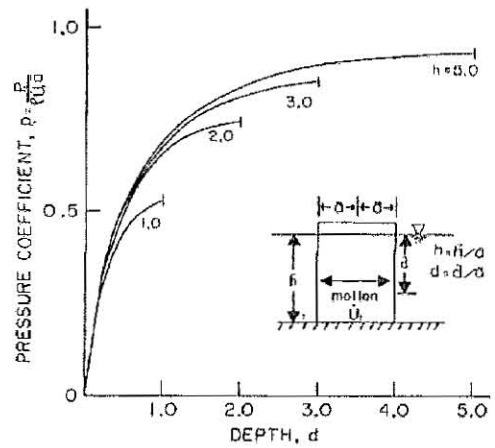


Fig. 11 - Pressure amplitude on meridian of a vertical cylinder.

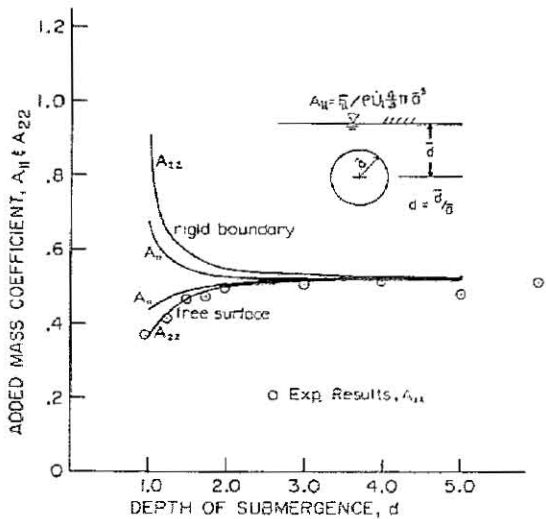


Fig. 12 - Added mass coefficient for a sphere in a fluid of infinite depth.

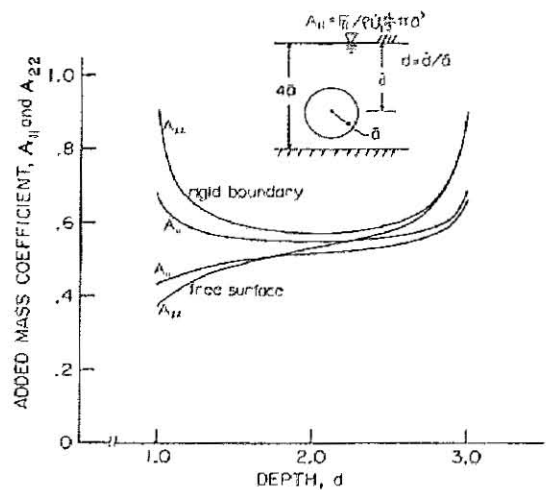


Fig. 13 - Added mass coefficient for a sphere for  $h = 4.0$ .

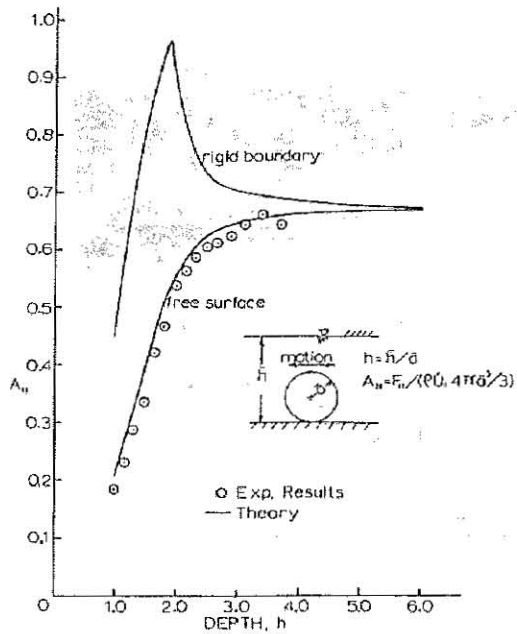


Fig. 14 - Added mass coefficient for a bottom mounted sphere.

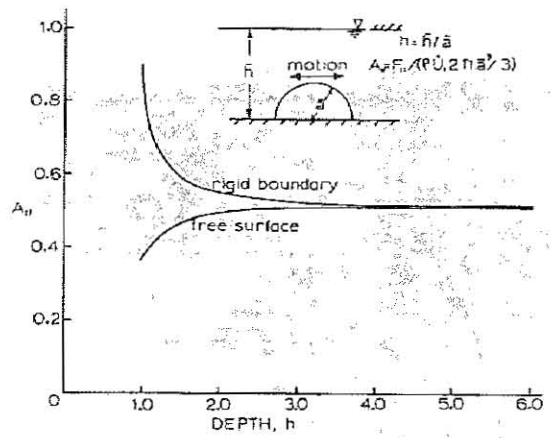


Fig. 15 - Added mass coefficient for a hemispherical vessel.

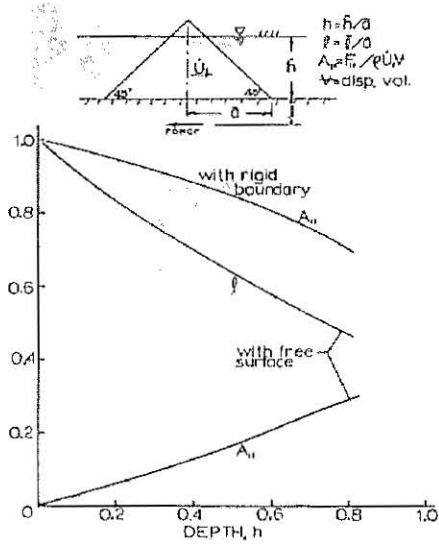


Fig. 16 - Added mass coefficient and line of action of horizontal force for a cone.

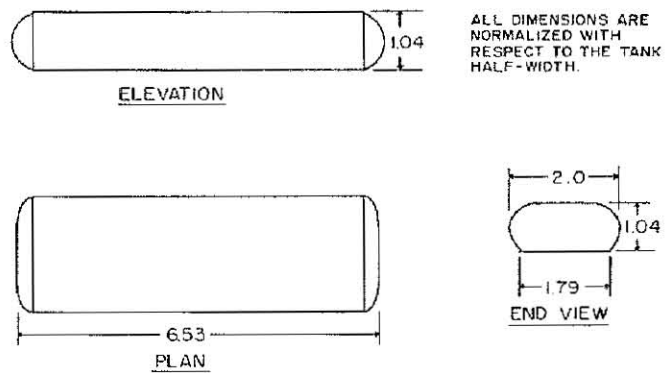


Fig. 17 - Submerged oil storage tank.

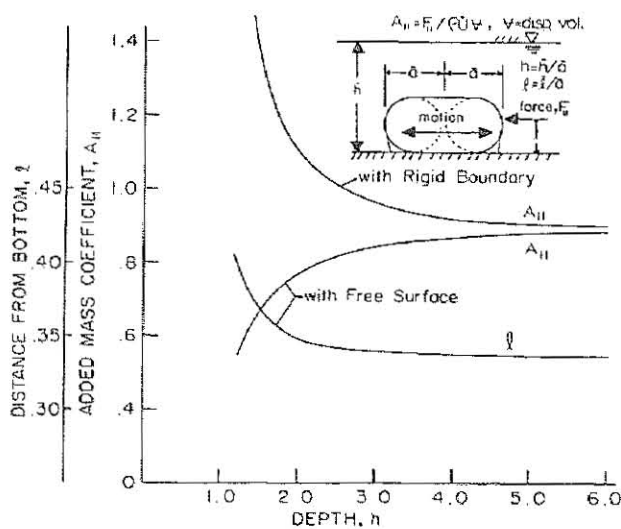


Fig. 18 - Added mass coefficient and effective line of action of hydrodynamic force for a submerged oil storage tank.